Indonesian Journal of Aerospace Vol. 21 No. 2 Desember 2023 : pp 133 – 146 (Pramana et al.)
DOI: 10.55981/ijoa.2023.272
https://ejournal.brin.go.id/ijoa/

A Study on Lug Structure at Fuselage - Wing Joint of an Unmanned Aerial Vehicle Using Finite Element Method

Nurhadi Pramana[1,a)], Fadli C. Megawanto[2], Chairunnisa[3], M. Ilham Adhynugraha[2], Agus Aribowo[2], Abian Nurrohmad[2], Andi Kuswoyo[4]

[1]*Research Center for Computing, BRIN, Indonesia*
[2]*Research Center for Aeronautics Technology, National Research and Innovation Agency, BRIN, Indonesia*
[3]*Research Center for Energy Conversion and Conservation, BRIN, Indonesia*
[4]*Faculty of Mechanical and Aerospace Engineering, Institut Teknologi Bandung, Indonesia*
Corresponding e-mail: nurh030@brin.go.id

Received: 08-02-2023 Accepted: 30-10-2023 Published: 31-12-2023

Abstract

Research on structural analysis of an unmanned aerial vehicle (UAV) is carried out. The primary material used in most structures is carbon composite. Having a high aspect ratio wing, the lugs connecting the wing and fuselage are likely to experience maximum forces during flight tests. In predicting the occurrence of deformation and stress, the finite element method is used by applying max./min. strain criteria to evaluate the structural integrity of composite wings due to the load applied on aluminum-based lugs. The evaluation shows that the current wing configuration has good structural integrity. An optimization approach is also carried out to obtain more optimum results.

Keywords: *UAV; lug; aluminum material; finite element; strain criteria*

Nomenclature

b	=	Wing Span, m
S	=	Wing Area, m^2
C_r	=	Root Chord, m
C_t	=	Tip Chord, m
AR	=	Aspect Ratio

1. Introduction

Over the last few decades, unmanned aerial vehicles (UAVs) have been employed for landscape monitoring and photogrammetry. From the point of view of lift production, there are two types of UAVs, i.e., fixed-wing and multi-rotor craft. For longer flight endurance, fixed-wing UAVs are more suitable for use, while for stable image capturing and easy vertical take-off and landing, multi-rotor ones are favorable [1, 2]. Multi-rotor UAVs require high-speed propeller rotation to produce lift but with the consequence of low aerodynamic efficiency. Conversely, fixed-wing UAVs have the advantages of a high lift-to-drag ratio with long stagnation time, high speed, and wide-range maneuvers [2].

Although UAV development projects are mostly for military purposes, there is an increase in the need for civilian fields including agriculture [3], environmental [4], fishery [5], and urban planning [6]. This variety of needs drives the rise of new designs of UAVs. One of the UAVs that has promising projections in the future is fixed-wing Medium Altitude Long Endurance (MALE) UAVs.

Design-wise, a fixed-wing UAV is built similarly to conventional fixed-wing aircraft. The airframe is made up of a mechanical structure that supports wings, fuselage, empennage, etc. The wing is the main structure in bearing the load before being transferred to the fuselage, it is necessary to know the strength of the lug in predicting the occurrence of

deformation and stress of the fuselage-wing lug. Hence a thorough analysis of wing design is required.

In the development of unmanned aerial vehicles, the aircraft's wings played a significant role without compromising flight performance and aerodynamics [7]. Elmeseiry et al. [8] stated that a medium UAV wingspan applies to UAVs between 2 and 10 m. Wandono et al. [9] found that a reinforced composite wing structure UAV with rib and double spar could meet the load factor regulation specified in CASR Part 23. Meanwhile, Romeo et al. [10] revealed that the solution for increasing the bending stiffness of an excellent structural wing could be represented by a precisely reinforced high-modulus carbon fiber leading edge; in addition, the main spar can be divided into sections that can be connected.

2. Methodology

The evaluation of grid independence was carried out and followed by the stress analysis. The shell surface model was used to simplify the process. The numerical results were compared to the material properties to determine the strength of the structure. Here the observation of metal and composite is done individually to study the effect of the loads applied towards both materials where the composite parts used with max/min strain criteria, while the metal parts employed von Mises criteria. In this study, boundaries were defined as fixed in every axial direction and placed on the hole of the lugs. The loads were along the span on a line representing the wing's center of pressure.

The effect of varying thicknesses of aluminum lugs toward overall wing structural integrity may fill the area's gap of knowledge. The influence of layer orientation of composite spar due to the metal-composite interaction is also proposed as the novelty of this research.

2.1. Related Works

Rumayshah et al. [11] applied the finite element method for structural analysis on the high altitude and HALE UAV. The results indicate that the initial configuration fails, as demonstrated by a Tsai-Wu failure criterion of 63.68 for composite components and a Von-Mises failure criterion of less than 1 for homogeneous parts for the entire model. The second iteration suggests a new configuration that includes material, ply orientation, and thickening in some areas. With a Tsai-Wu failure criterion of 0.865, this innovative structural structure is proven successful against the given loads.

The work of Solob et al. [12] is based on the application of the extended finite element method (XFEM) to the determination of stress intensity factors (SIFs) in the case of a fatigue crack in the wing-fuselage attachment lug of a light aerobatic aircraft. The presence of a through-the-thickness crack at the attachment lug hole is not permitted because its growth due to high dynamic loads is typically rapid and can have disastrous consequences.

Kumar et al. [13] investigated various materials for stress analysis and maximum tensile stress in one of the lug holes on wing-fuselage attachment brackets. As a result, the maximum equivalent stress observed at the midpoint of the root section for aluminum alloy, and titanium alloy, and because it is lower than the yield stress, Carbon Fibre Reinforced Polymer (CFRP) is considered safe.

Boljanović et al. [14] analyzed the fatigue behavior of failure critical pin-loaded lug with a through-the-thickness crack at the hole including stress analysis and the residual life estimation. The fatigue estimations show that the width-diameter ratio, height of the lug head, and thickness can significantly affect the residual strength of the pin-loaded lug under cyclic loading. For various geometry and thicknesses, the phenomenon of crack length versus several loading cycles to failure for the lug with a through-the-thickness crack has the same trend.

2.2. Problem Definition

The development of a fixed-wing UAV is an existing government project related to this research. A UAV with a medium altitude long endurance mission demands a high wing aspect ratio to assure long flight endurance and low drag, which became the feature of the project design. The UAV has a 16 m wingspan, and most of its structures are carbon composite. At the wing lug location, there is a concern that is the subject of this study. The wing-to-body connection requires an arrangement that can bear the wing's loads before being passed to the body. Every effort is made to increase the wing lug's capacity to provide a lightweight, simple-to-manufacture, simple-to-assemble construction that can handle each load that may be encountered.

The configuration structure is shown in Fig. 2-1. The wing constitutes five sections. The wing box is reinforced with several carbon fiber ribs along the wing span and there are two spars c-shape carbon fiber, the ends of both are connected by aluminum lugs to attach to the fuselage, while the leading edge is composed of carbon fiber, and joined at the front spar.

This UAV has a maximum weight of 1300 kg and a range of 250 km at 7300 m altitude. Table 2-1 displays the UAV wing characteristics and measurements. The design and structural analysis of the aluminum wing lug using the finite element model is the main subject of the current study. The numerical analysis forecasts how a wing lug structure will react to a specific load. Due to the symmetry of the wing geometry, the simulation was done for half of the wing span to speed up computation. The output was employed to evaluate the strength of the structure against the loads applied, which were the superposition of lift and weight distributed along the wing.

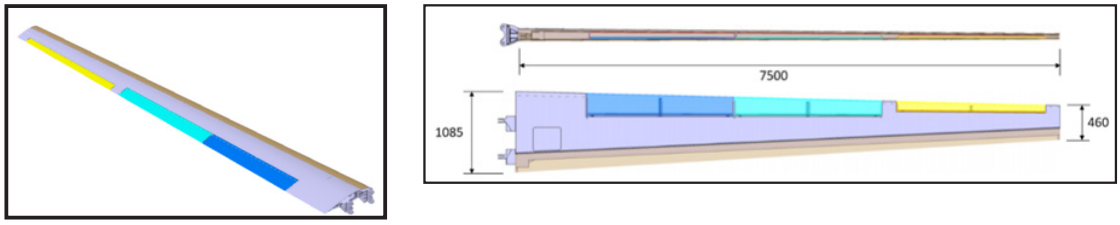

(a) (b)

Figure 2-1: Wing, a) configuration UAV, b) dimension in mm

Table 2-1: Wing Specifications

b	m	7.5
S	m^2	45
C_r	m	1.085
C_t	m	0.46
AR	-	20

2.3. Method

SIMULATION SETUP

The Finite Element Method (FEM), which divides the wing into finitely small components, is one method for analyzing the structural response. These minor components are then examined to find a solution for the entire area. These little pieces are known as elements with nodes connecting them, obtained from meshwork. The lamination feature can be modeled in the finite element approach, allowing customization of the material properties and further processing in the static structural analysis.

Regulation

The design of this UAV complies with CASR Part 23 [15]. Strength requirements are specified in terms of limit loads (the maximum loads to expect in operation) and ultimate loads (limit loads multiplied by prescribed safety factor). Unless otherwise provided, the prescribed loads are limit loads, and the safety factor is 1.5.

Wing Design

Figure 2-2 shows the half-sided wing proposed design for the UAV. The wing is designed with two spars (front and rear). There are several ribs to maintain the shape of the wing. Meanwhile, the connection between the wing and the fuselage is a lug system.

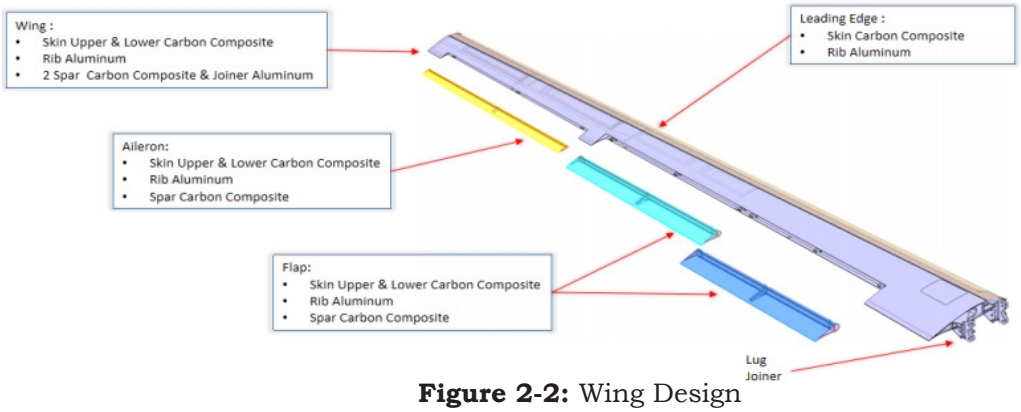

Figure 2-2: Wing Design

Meshing

The model in this study uses the shell surface type, which consists of quad elements with four nodes (quad4). The flange parts, i.e. beam and rib, are modeled as 1D bar elements. This approach reduces the computational time. To get the desired shape of the flange, section profiles were defined on each bar element as shown in Fig. 2-3.

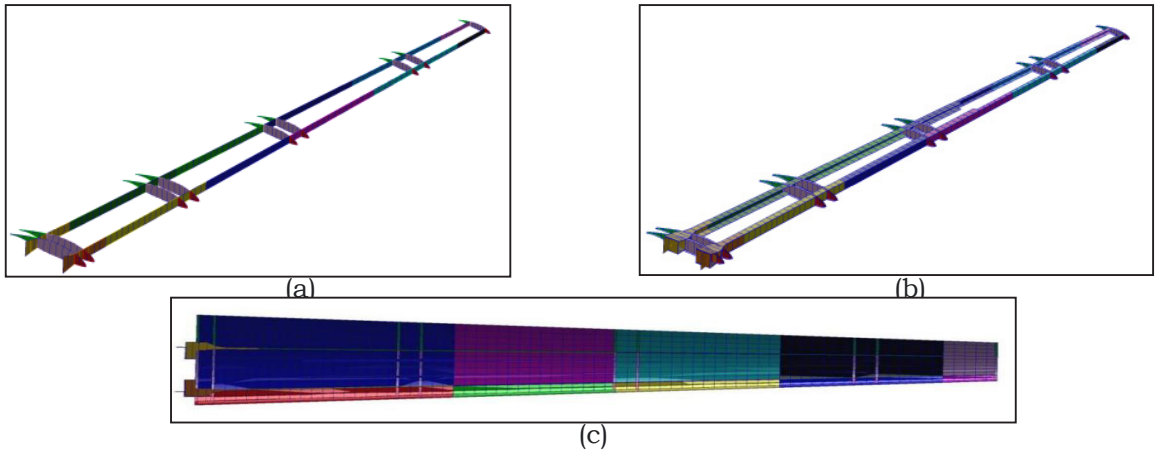

Figure 2-3: a) Beam and rib without 1D bar section profile, b) Beam and rib with 1D bar section profile with visualization, c) Wing meshing

To ensure that mesh quality was proper, Fig. 2-4 shows a few configurations of mesh number were made. Therefore, there were four sets of different configurations, which were varied by the number of elements. From the most coarse to the most refined configuration, total element numbers 2480, 5244, 10120, and 19128 were used respectively.

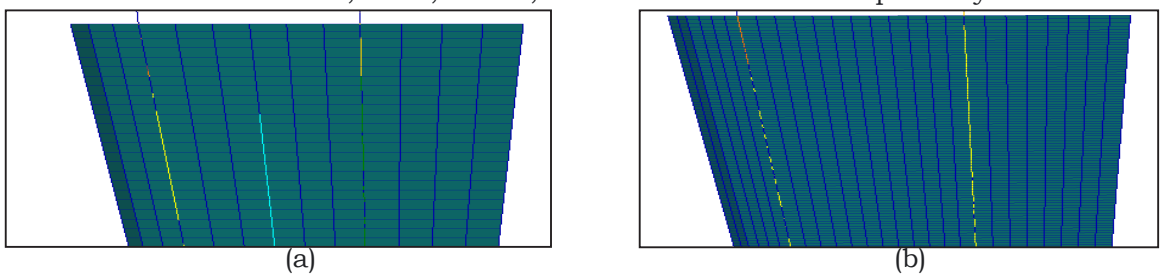

Figure 2-4: Comparison between a) the most coarse and, b) the most refined configuration

In order to verify its convergence, a simple load and boundary condition were applied to all configurations. The load, in the form of a uniform pressure with a value of 500 MPa, was applied to the lower surface area, while the boundary condition was set to fix the lug elements. As a result, the von Mises stress can be observed below for all configurations:

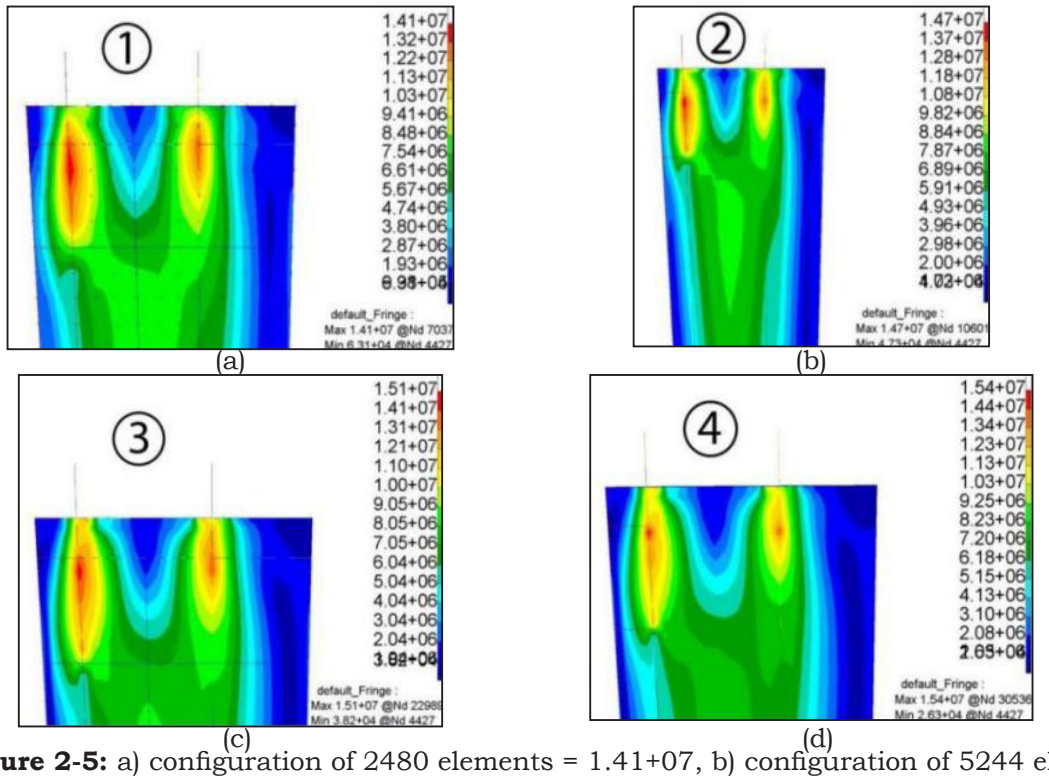

Figure 2-5: a) configuration of 2480 elements = 1.41+07, b) configuration of 5244 elements = 1.47+07, c) configuration of 10120 elements = 1.51+07, d) configuration of 19128 elements = 1.54+07

Based on the above results, it is evident that the 3rd and 4th configurations produce similar outcomes, despite the 4th configuration having almost twice as many elements as the 3rd configuration. Therefore, to reduce the computational load, the 3rd configuration was selected for the simulation.

Load and Boundary Condition

The load on the wing follows the Schrenk method of load distribution and was applied to the model using nodal forces. The nodes were positioned at the 50% wing chord, starting with the first node at 1000 WSTA and progressing spanwise with a distance of 500 mm between each node. In this simulation, pins are utilized as boundary conditions, restricting the translation of the nodes in the x, y, and z directions while allowing rotation in those directions. These boundary conditions represent bolts in the actual scenario. The applied loads and limit conditions are presented below.

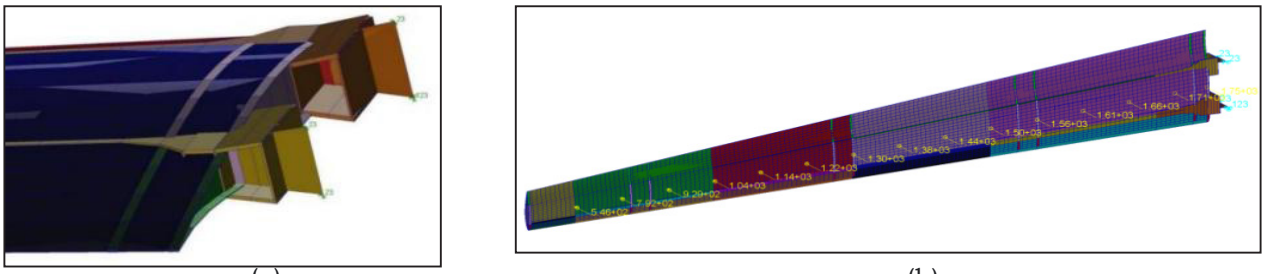

Figure 2-6: a) Boundary Condition, b) Wing Load with Schrenk Distribution

Material Properties

Regarding the structural design requirements, composite materials are utilized in almost all wing components. Due to the particular characteristics of composite materials, especially their unique damage mechanisms, many specific requirements for their structural integrity differ from those for metal structures. Here are the mechanical properties of the material [16, 17]:

Table 2-2: Mechanical Property of wing

Material		**Properties**		**Unit**
UD Tape 8552 IM7	Elastic Modulus	E11 (Compression Dry 25 deg)	150000	MPa
	Elastic Modulus	E22 (Dry 25 deg)	12000	
	Poisson ratio	v12	0,316	
	Shear modulus	G12	1930	
	Density	(ETW-->Elevated Temperature/Wet)	1,57E-06	kg/mm^3
	Strain Allowable	X_{ε}^{t}	0.016*	
		X_{ε}^{c}	0.006**	
HRH10-3.2-48	Elastic Modulus	E	138	MPa
	Density	pro	4,80E-08	kg/mm^3
Material	**Yield Strength**	**Tensile strength**	**Modulus Elasticity**	**Density**
		MPa		**Ton/mm²**
AL 7050 T7541	469	524	71000	2,80E-09
AL 2A12	205	470	71000	2,80E-09

Note: - Originally, the allowable strain data was obtained by technical specification from the vendor. But, this is subject to change due to how manufacturers handle the process. Also, composite is well known for the difficulty of the manufacturing process, which will imply plenty of imperfection to its final product when it's getting cured. Regarding that matter, in this simulation, the factor of 2 was applied to divide the allowable strain value over.

*Obtain from vendor material specification

**Obtain from reference [18]

Stacking Sequence

Composite laminates consist of two or more layers arranged in a unidirectional manner, with the fibers oriented in the same or different directions. These layers, called plies, can be composed of the same or different materials and have varying thicknesses. The stacking sequence of the plies is expressed in the table below:

When utilizing a stacking sequence of 0°/45°/90°, according to the Hart-Smith modified maximum strain failure criterion, the strain failure for a laminate can be represented by an envelope, as shown in Figure 2-7. Unlike the original criteria, which do not consider the effect of fiber shear off, this modification addresses the issue by truncating the original failure envelope with a 45° sloping line passing through the greater strain-to-failure (in this case, tension) for a unidirectional lamina subjected to uniaxial stress. This truncation effectively imposes a limit on the in-plane shear strength of matrix-dominated laminates. [19].

Table 2-3: Stacking sequence

Stacking Arrangement for Wing Skin							
Ply	**Material**	**Joiner**	**Zone.1**	**Zone.2**	**Zone.3**	**Zone.4**	**Zone.5**
Ply.1	UD_Tape_IM7	45	45	45	45	45	45
Ply.2	UD_Tape_IM7	90	90	90	90	90	90
Ply.3	UD_Tape_IM7	-45	-45				
Ply.4	UD_Tape_IM7	0	0	0	0		
Ply.5	UD_Tape_IM7	45					
Ply.6	UD_Tape_IM7	90					
Ply.7	UD_Tape_IM7	-45					
Ply.8	UD_Tape_IM7	0	0	0	0	0	
Ply.9	UD_Tape_IM7	45	45				
Ply.10	UD_Tape_IM7	-45					
Ply.11	UD_Tape_IM7	0					
Ply.12	UD_Tape_IM7	-45	-45	-45	-45	-45	-45
Ply.13	UD_Tape_IM7	90	90	90			
Ply.14	UD_Tape_IM7	45	45	45			
Ply.15	UD_Tape_IM7	0	0	0	0	0	0
Symmetry Stacking							

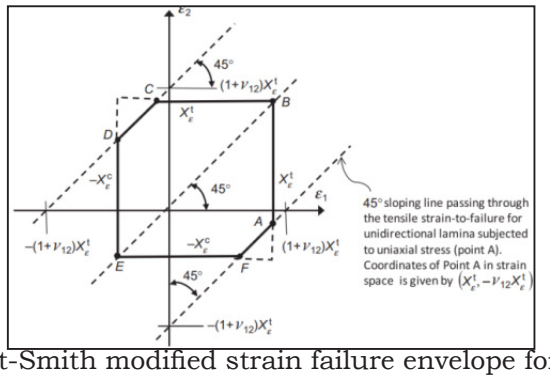

Figure 2-7: Hart-Smith modified strain failure envelope for a lamina [19]

Looking at Fig. 2-7, shear strain allowable is limited at point A. Therefore, the shear strain allowable could be defined the same as the coordinate of point A:

$$S_\varepsilon = \nu_{12} X^t_\varepsilon \quad (2\text{-}1)$$

Where, S_ε = Shear Strain Allowable
υ_{12} = poisson's ratio
X^t_ε = Tensile Strain Allowable

Therefore, the shear strain allowable value is as mentioned:

$S_\varepsilon = 0.316 \; x \; 0.16$

$S_\varepsilon = 0.005$

Based on the distortion energy theory, yielding occurs when the distortion strain energy per unit volume is equal to or greater than the distortion strain energy per unit volume for yield in simple tension or compression of the same material.

$$U_s = \frac{1}{12G}[(\sigma_I - \sigma_{II})^2 + (\sigma_{II} - \sigma_{III})^2 + (\sigma_{III} - \sigma_I)^2] \quad (2\text{-}2)$$

When simple tension fails, the shear or distortion strain energy per unit volume is equal to σ $\sigma_I = \sigma_Y$, $\sigma_{II} = \sigma_{III} = 0$. Hence from eq. 2-2

$$U_s = \frac{\sigma_Y^2}{6G} \quad (2\text{-}3)$$

The von Mises criteria state that failure occurs when U_s, given by Eq. 2-2, reaches the value of U_s, given by Eq. 2-3 i.e., when

$$(\sigma_I - \sigma_{II})^2 + (\sigma_{II} - \sigma_{III})^2 + (\sigma_{III} - \sigma_I)^2 = 2\sigma_Y^2 \quad (2\text{-}4)$$

For a two-dimensional stress system in which $\sigma_{III}=0$, Eq. 2-4 becomes

$$\sigma_I{}^2 + \sigma_{II}{}^2 - \sigma_I\sigma_{II} = \sigma_Y^2 \quad (2\text{-}5)$$

For pure tension, $\sigma\sigma_{II} = -\sigma - \sigma_P$, $\tau\tau = \sigma\sigma_I$

$$\sigma_Y = \sqrt{3\sigma_I} = \sqrt{3\tau} \; or \; \tau_Y = \frac{1}{\sqrt{3}}\sigma_Y = 0.577\sigma_Y \quad (2\text{-}6)$$

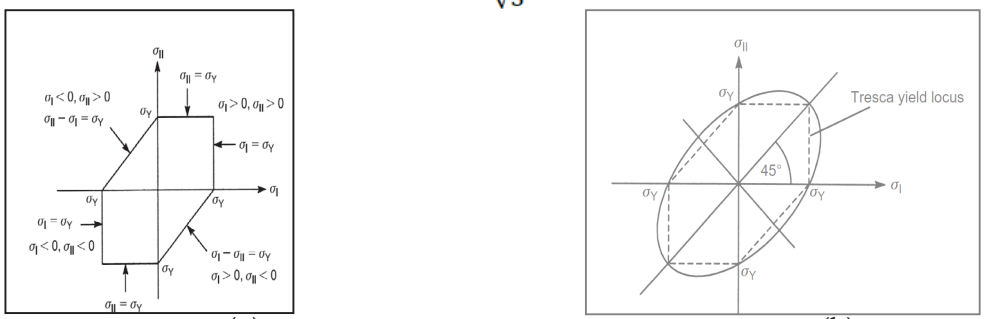

Figure 2-8: (a) Yield locus for the Tresca theory of elastic failure, and (b) Yield locus for the von Mises theory [20]

For a two-dimensional stress system, the shear strain energy (von Mises) hypothesis is represented by Eq. 2-5. This equation can be demonstrated to form an ellipse, as depicted in Figure 2-8, with its major and minor axes inclined at a 45° angle to the axes of σ_I and σ_{II}. Additionally, it can be shown that the six corners of the Tresca yield locus coincide with the points where the ellipse intersects, indicating that these locations yield the same results for both theories. However, it is important to note that the Tresca theory is more conservative since it predicts failure for combinations of σ_I and σ_{II} that the von Mises theory does not.

3. Result and Analysis

Using the simulation methods outlined above, Where the detailed Finite Element analysis was done on the wing, the numerical simulation results are presented as follows.

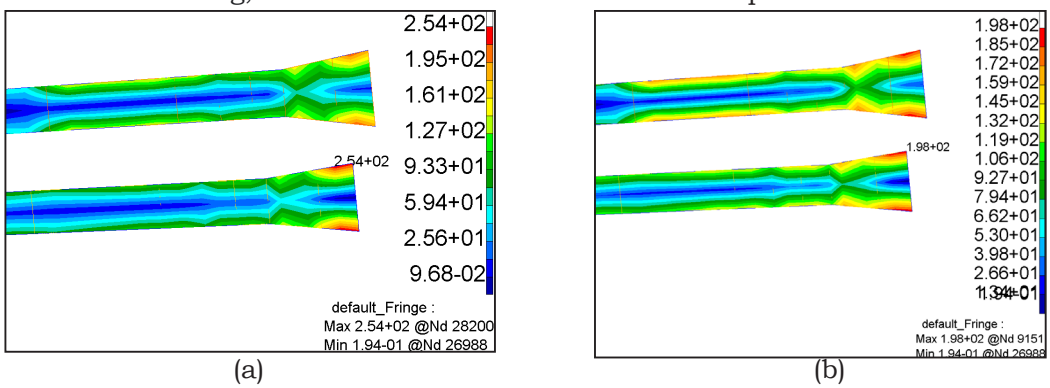

Figure 3-1: Lug Metal von mises: (a) Former Iteration, (b) Final Iteration

The initial condition of the fuselage-to-wing lug exhibits a von Mises yield value of 254 MPa. To improve the results, further iterations were performed by thickening the lug. After several iterations, the von Mises failure criterion for the lug indicates that the lug structure is now considered safe. In Figure 3-1, the maximum yield value gained from the optimization of the lug is 198 MPa. However, it's worth noting that the required yield strength condition for the material used, in this case AL 2A12, is 205 MPa. Another factor to consider is the effect of the optimization process on the mass of the lug. In the former iteration, the total mass of the front spar and rear spar was 14.1 kg (with front thickness of 24mm and rear thickness of 20mm), while in the final iteration, the total mass increased to 15 kg (with front thickness of 27mm and rear thickness of 25mm).

To ensure the overall safety of the wing, it is crucial to examine both the compression strain and tension strain. The optimization results of the wing-forming layer composition are displayed in Figure 3-2. The concept behind this optimization is to reverse the layer orientation to reinforce the sections experiencing high loads. These findings indicate that by optimizing the composition of the wing-forming layer, the compressive strain value can be enhanced. Consequently, based on these optimization results, it can be concluded that the skin and spar of the wings are secure when subjected to loads in the lug area.

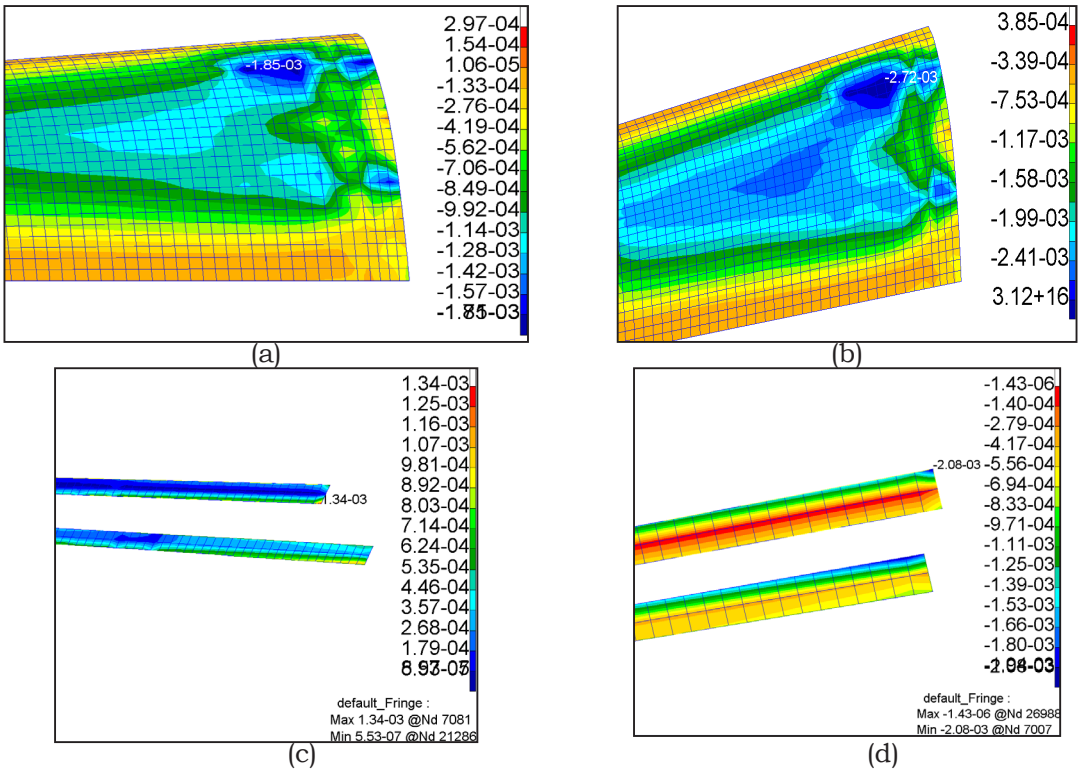

Figure 3-2: Compression Strain: Skin Composite (a) non-optimized (1850 με), (b) Optimized (2720 με) Spar Composite: (c) non-optimized (1340 με), (d) Optimized (2080 με)

In addition to the tension strain value, Figure 3-3 illustrates that the optimization of the skin and spar has effectively increased the tension strain, ensuring that the wing can withstand the tensile forces. Additionally, the shear strain results are displayed in Figure 3-4.

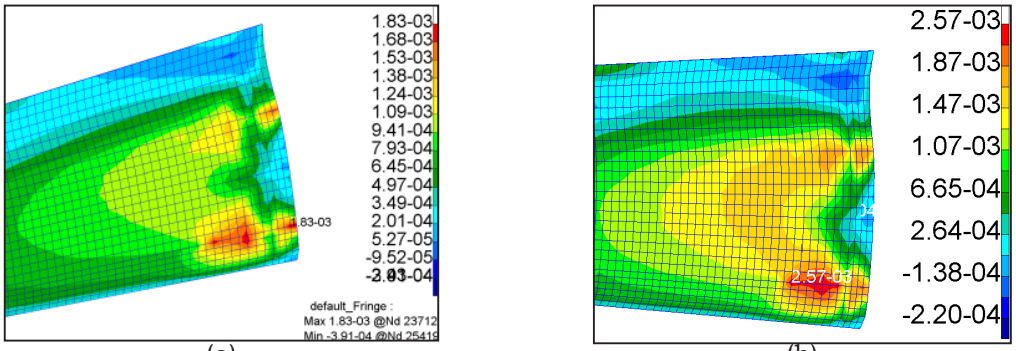

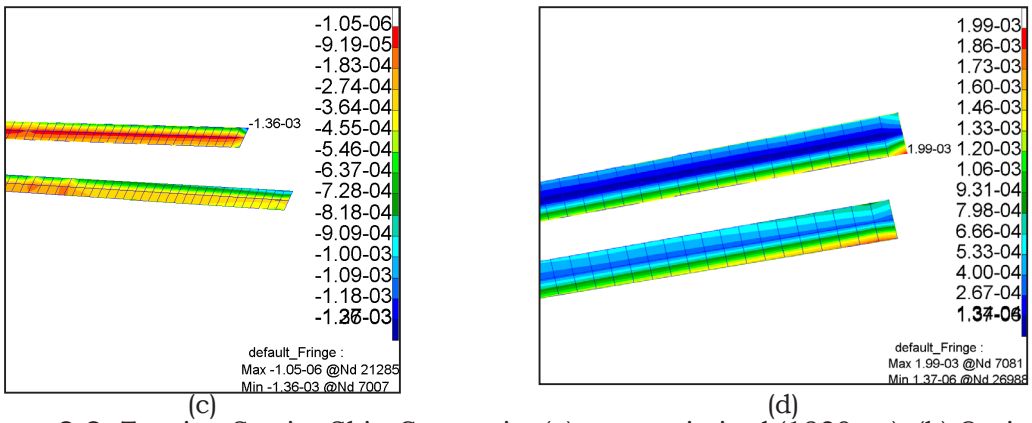

(c) (d)

Figure 3-3: Tension Strain: Skin Composite (a) non-optimized (1830 με), (b) Optimized (2570 με) Spar Composite (c) non-optimized (1360 με), (d) Optimized (1990 με)

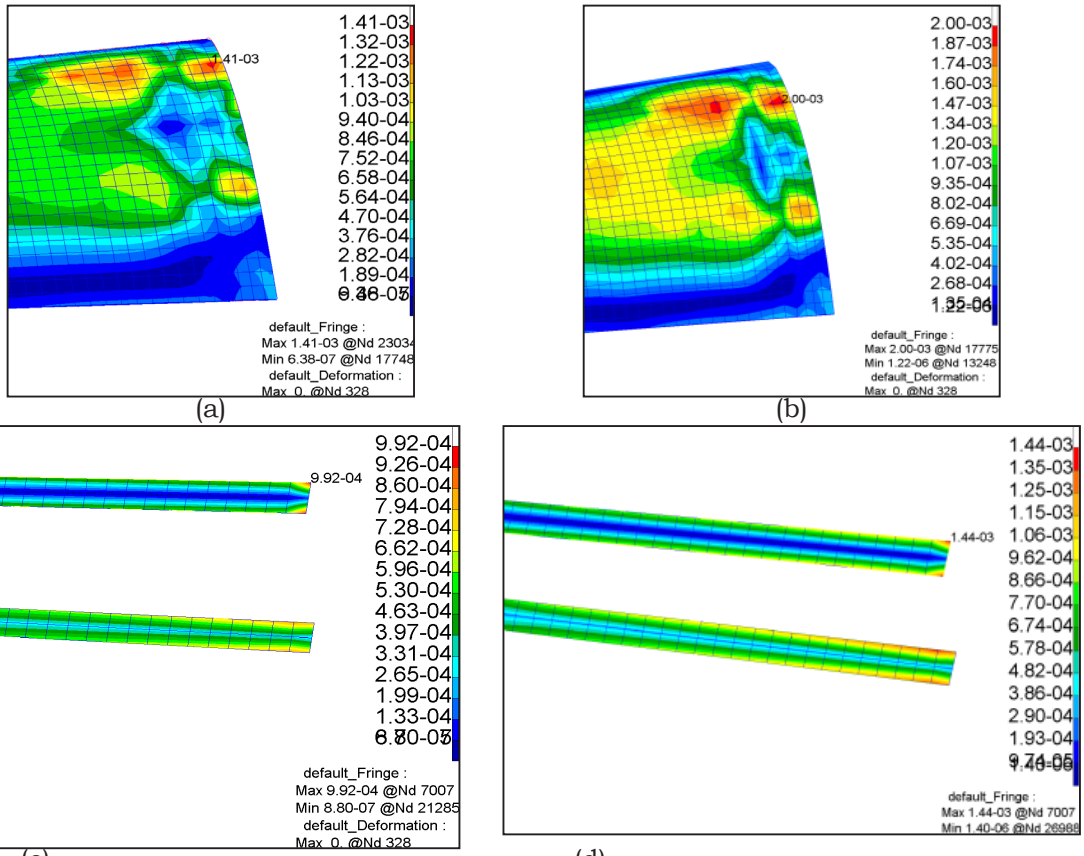

(a) (b)

(c) (d)

Figure 3-4: Shear Strain: Skin Composite (a) non-optimized (1410 με), (b) Optimized (2000 με) Spar Composite (c) non-optimized (992 με), (d) Optimized (1440 με)

Margin safety is a value to measure structure safety level when the load is applied. The common formula is used, which is:

$$\text{M. S.} = \frac{\text{Material Allowable}}{\text{Stress Occured}} - 1$$

For composite parts, an additional safety factor of 2 is applied due to the potential imperfections that may occur during the manufacturing process. Therefore, the material allowable values for each load direction are as follows: $X_{\varepsilon}^{t} = 0.008 \approx 8000\mu\varepsilon$; $X_{\varepsilon}^{c} = 0.003 \approx 3000\mu\varepsilon$; $S_{\varepsilon} = 0.0025 \approx 2500\mu\varepsilon$. The result of the numerical compression, tension, and shear stress calculation is shown in table 3-1 below:

Table 3-1: Margin of safety

	Compression		Tension		Shear		Material
	Non-Optimized	Optimized	Non-Optimized	Optimized	Non-Optimized	Optimized	
Skin	0.62	0.1	3.37	2.11	0.77	0.25	UD Tape 8552 IM7
Spar	1.23	0.44	4.88	3.02	1.52	0.73	UD Tape 8552 IM7
	Von Mises						
	Former Iteration (Fail)			Final Iteration			
Lug	-0.2			0.03			AL 2A12

From the optimization results of the design, further comparisons were made with similar cases. A study conducted by Frulla & Cestino [21] involved the design, manufacturing, and testing of High Altitude Long Endurance (HALE) aircraft wings. This case exhibited similarity in terms of wing span length. The parameter compared was the maximum deflection occurring at the wing tip. From Figure 3-5, it can be observed that the maximum deflection value at the wing tip, with the optimized lug, was 627 mm, whereas the maximum deflection value for the HALE wing was 764 mm, as seen in Figure 3-6. This result is acceptable considering that the span length of the optimized structure is 16 meters, while the span length of the HALE wing used as a reference is 24 meters.

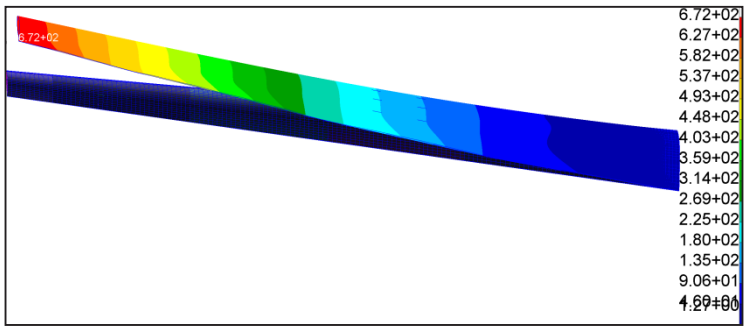

Figure 3-5: The deformation value at the wing tip is 672mm

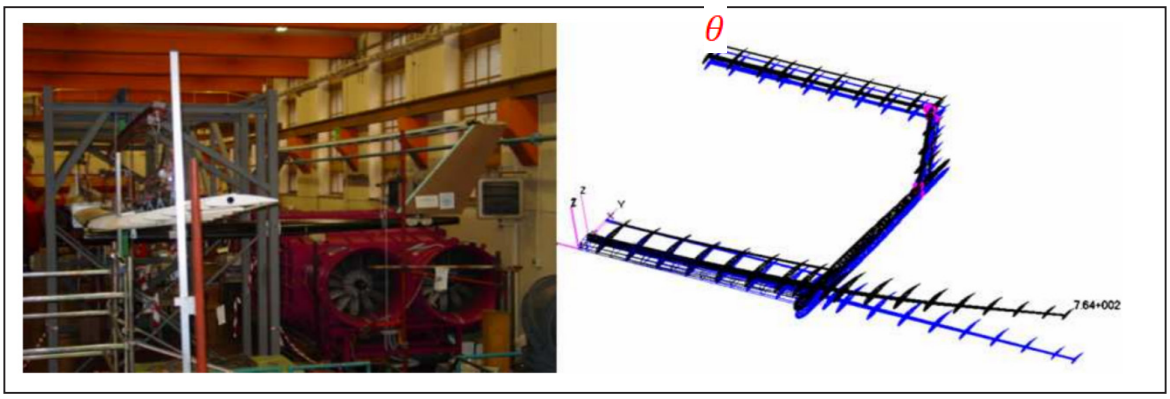

Figure 3-6: FE and Experimental results at D-D1 condition

4. Conclusions

The Finite Element Method was employed to conduct a numerical investigation of the lug structure in the UAV's fuselage-wing joint. Current studies on fuselage-wing lugs demonstrate satisfactory agreement with benchmark models. Prior to conducting the global finite element method, a mesh convergence test analysis was performed to determine the optimal mesh size (GFEM).

The UAV wing consists of a laminated composite material with aluminum utilized in the lug. The applied load in this study adheres to the regulations outlined in CASR Part 23. Various types of loads act upon the lug, including aerodynamics, inertia, attachment force, and fitting force.

The fuselage-wing lug study demonstrates the results of optimizing the compression and tension strain values on the wing's spar and skin. These optimizations indicate that the wing structure configuration can withstand the imposed load. However, additional optimization is required for other components, such as the rib and the lug's shape, which should be investigated further.

Acknowledgments

This work is supported by the project "Topology optimization of MALE UAV fuselage structure with a numerical approach based on finite element method" No.6/III/HK/2022 under the grant of research Organization for Aeronautics and Space of National Research and Innovation Agency (BRIN), Bogor, Indonesia.

Contributorship Statement

N.P. and F.C. conceived of the presented idea and carried out the simulations. M.I. verified the analytical methods. A.A. helped supervise the funding of this project and was in charge of overall planning. C. and A.N. wrote the manuscript with support from A.K. All authors discussed the results and contributed to the final manuscript.

References

Boon, M.A., 2017. Comparison of a fixed-wing and multi-rotor UAV for environmental mapping applications: A case study.

Zhou, M., Zhou, Z., Liu, L., Huang, J. and Lyu, Z., 2020. Review of vertical take-off and landing fixed-wing UAV and its application prospect in precision agriculture. International Journal of Precision Agricultural Aviation, 3(4).

Kim, J., Kim, S., Ju, C. and Son, H.I., 2019. Unmanned aerial vehicles in agriculture: A review of perspective of platform, control, and applications. IEEE Access, 7, pp.105100-105115.

LATICI, T., 2019. Civil and military drones: Navigating a disruptive and dynamic technological

ecosystem.

Provost, E.J., Butcher, P.A., Coleman, M.A., Bloom, D. and Kelaher, B.P., 2020. Aerial drone technology can assist compliance of trap fisheries. Fisheries management and ecology, 27(4), pp.381-388.

Xu, C., Liao, X., Tan, J., Ye, H. and Lu, H., 2020. Recent research progress of unmanned aerial vehicle regulation policies and technologies in urban low altitude. IEEE Access, 8, pp.74175-74194.

Structural Analysis of UAV Airframe by using FEM Techniques: A Review

Elmeseiry, N., Alshaer, N. and Ismail, T., 2021. A detailed survey and future directions of unmanned aerial vehicles (uavs) with potential applications. Aerospace, 8(12), p.363.

Wandono, F.A. and Adhitya, M., 2020, May. Finite element analysis for composite wing structure of the maritime surveillance unmanned aerial vehicle. In AIP Conference Proceedings (Vol. 2227, No. 1, p. 020029). AIP Publishing LLC.

Romeo, G., Frulla, G. and Cestino, E., 2007. Design of a high-altitude long-endurance solar-powered unmanned air vehicle for multi-payload and operations. Proceedings of the Institution of Mechanical Engineers, Part G: Journal of Aerospace Engineering, 221(2), pp.199-216.

Rumayshah, K.K., Prayoga, A. and Moelyadi, M.A., 2018, April. Design of high-altitude long endurance UAV: Structural analysis of composite wing using finite element method. In Journal of Physics: Conference Series (Vol. 1005, No. 1, p. 012025). IOP Publishing.

Solob, A., Grbović, A., Božić, Ž. and Sedmak, S.A., 2020. XFEM based analysis of fatigue crack growth in damaged wing-fuselage attachment lug. Engineering Failure Analysis, 112, p.104516.

Kumar, A. S., & Raju, D. (2020). Static Structural Linear Analysis of Fuselage Lug Joint Bracket for a Transport Aircraft with Mid Wing Configuration. International Research Journal of Engineering and Technology

Boljanović, S., & Maksimović, S. (2017). Fatigue damage analysis of wing-fuselage attachment lug. Procedia Structural Integrity, 5, 801–808.

Ministry of Transportation, Civil Aviation Safety Regulation (CASR) Part 23 Amdt 2, (Ministry of Transportation, Jakarta, 2014).

Marlett, K., Ng, Y. and Tomblin, J., 2011. Hexcel 8552 IM7 unidirectional prepreg 190 gsm & 35% RC qualification material property data report. National Center for Advanced Materials Performance, Wichita, Kansas. Test Report CAM-RP-2009-015, Rev. A, pp.1-238.

Hexcel corporation product data sheet, 2020. Hexcel 8552. USA

Wu, W., Wang, Q., & Li, W. (2018). Comparison of tensile and compressive properties of carbon/glass interlayer and intralayer hybrid composites. Materials, 11(7), 1105.

Wang, C. H., & Duong, C. N. (2015). Bonded joints and repairs to composite airframe structures. Academic Press.

Megson, T.H.G. 2019. Structural and Stress Analysis (Fourth Edition). Butterworth Heineman: Pages 423-466

Frulla, G., & Cestino, E., Design, manufacturing and testing of a HALE-UAV structural demonstrator. Composite Structures 83 (2008): Pages143-153